Single-Shot Ternary Readout of Two-Electron Spin States in a Quantum Dot Using Spin Filtering by Quantum Hall Edge States

H. Kiyama, T. Nakajima, S. Teraoka, A. Oiwa, and S. Tarucha

Phys. Rev. Lett. **117**, 236802 — Published 29 November 2016

DOI: 10.1103/PhysRevLett.117.236802

Single-shot ternary readout of two-electron spin states in a quantum dot using spin filtering by quantum Hall edge states

H. Kiyama,[1,*] T. Nakajima,[2] S. Teraoka,[3] A. Oiwa,[1] and S. Tarucha[2,3]

[1] *The Institute of Scientific and Industrial Research, Osaka University, 8-1, Mihogaoka, Ibaraki-shi, Osaka 567-0047, Japan*

[2] *Center for Emergent Matter Science, RIKEN, 2-1 Hirosawa, Wako-shi, Saitama 351-0198, Japan*

[3] *Department of Applied Physics, The University of Tokyo, 7-3-1 Hongo, Bunkyo-ku 113-8656, Japan*

(Dated: November 15, 2016)

We report on the single-shot readout of three two-electron spin states—a singlet and two triplet substates—whose z-components of spin angular momentum are 0 and +1, in a gate-defined GaAs single quantum dot. The three spin states are distinguished by detecting spin-dependent tunnel rates that arise from two mechanisms: spin filtering by spin-resolved edge states and spin-orbital correlation with orbital-dependent tunneling. The three states form one ground state and two excited states, and we observe the spin relaxation dynamics among the three spin states.

PACS numbers: 73.63.Kv, 72.25.Dc, 72.25.Hg, 73.43.-f

Readout of electron spins in a quantum dot (QD) is a key ingredient in spin-based quantum information processing. There have already been some reports on the single-shot spin readout [1–7], in which spin-dependent single-electron tunneling events are detected in real time. The spin readout is normally binary with, for example, spin-up and spin-down substates [1–3], or singlet and triplet spin states [4–7], and applied to qubits. However, instead of these qubits, joint states of d-level systems with $d > 2$, or "qudits", are considered to have advantages, such as reduced resource requirements [8] and simplified quantum gates [9]. In addition, studies on qudits offer intriguing physics of multi-level entanglement, coherence, and relaxation. In this context, single-shot readout of multiple quantum states would be very important. However, it has not yet been reported for electron spins in QDs, despite the fact that multi-electron spins intrinsically provide a multi-level system used for qudits and that QDs are good platform for investigating spin physics and constructing large-scale qudit-architecture.

One way to read out the multiple spin states in a QD is to detect tunnel rates between the dot and the contact lead, depending on the multiple spin states. This may be realized by simultaneously utilizing several spin-dependent tunneling mechanisms. A tunnel-rate-selective binary spin readout has been demonstrated by utilizing the combined effect of spin-orbital correlation and orbital-dependent tunneling (the orbital effect) [4–6]. In this readout, the two-electron spin state is identified as either a singlet or triplets. When expanding this orbital effect, ternary spin readout may be possible with another mechanism that distinguishes one of the triplets from the rest.

For this purpose, the spin filtering by spin-resolved edge states formed in a two-dimensional electron gas (2DEG) near a QD [10] is useful. The tunnel coupling between the QD and the edge states is stronger for spin-up electrons than for spin-down electrons because the spin-up edge state is closer than the spin-down edge state to the dot. In this Letter, we observe the spin filtering in real-time for the first time, by a quantum point contact (QPC) charge sensor near the dot. Then, we demonstrate the single-shot ternary readout of two-electron spin states, a singlet (S) and two triplets having the z-components of the spin angular momentum $S_z = 0$ (T_0) and +1 (T_+), using the edge-state spin filtering and the orbital effect.

The experiments are performed for a gate-defined single QD with a QPC charge sensor [Fig. 1(a)] in a GaAs/AlGaAs heterostructure with a 2DEG of density $3 \times 10^{11}\mathrm{cm}^{-2}$ and mobility $1 \times 10^{6}\mathrm{cm}^2/\mathrm{V\,s}$, located 100 nm beneath. The tunnel coupling between the QD and the left reservoir is set to be negligibly small, such that electrons dominantly tunnel between the QD and the right reservoir instead. To improve the spin-filtering efficiency, we apply a negative voltage to gate MR [see Fig. 1(a)] to decrease the spatial gradient of the electrostatic potential near the tunnel junction, thereby increasing the spatial separation of adjacent edge states [11]. All measurements are performed with the device placed in a dilution refrigerator with a base temperature of 80 mK and an electron temperature of 160 mK under a magnetic field tilted by 30° from the 2DEG plane to increase the inter-edge state separation with larger Zeeman splitting. In this work, we apply the out-of-plane component, $B_\perp = 1.5$ T, at which the spin filtering is most efficient [12], because the spin-resolved edge states are well defined and the transport through excited states of the QD is inefficient [11, 21].

First, we observe the spin filtering via real-time charge sensing. Figure 1(b) shows the real-time trace of the change in the current through the QPC, ΔI_{QPC}, measured for the transition between the two-electron ($N = 2$) state and the three electron ($N = 3$) state, with a bias voltage of 0.2 mV and a bandwidth of 10 kHz. We define the empty and filled times for the dot as the lengths of

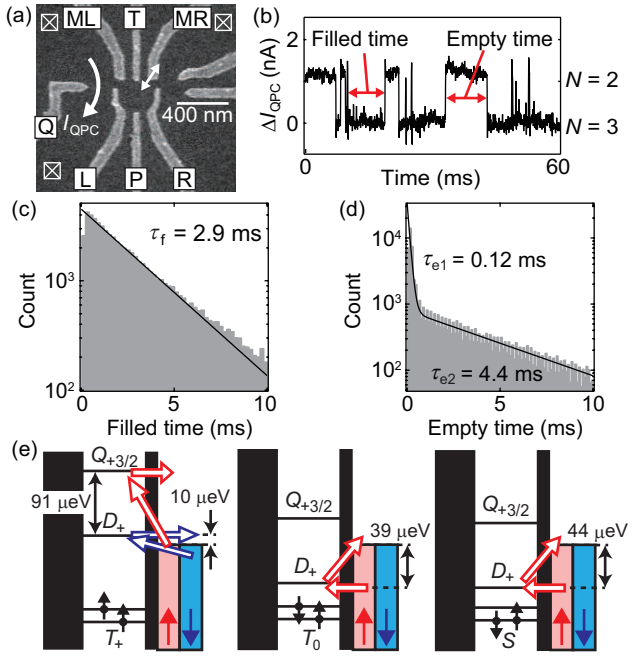

FIG. 1. (a) Scanning electron micrograph of the device. (b) Real-time trace of $\Delta I_{\rm QPC}$ measured for the transitions between the $N = 2$ and 3 states. (c) Histogram of the filled time, showing a single exponential distribution with a time constant of $\tau_{\rm f} = 2.9$ ms. (d) Histogram of the empty time, showing a double exponential distribution with time constants of $\tau_{\rm e1} = 0.12$ ms and $\tau_{\rm e2} = 4.4$ ms. (e) Energy level diagrams for the transition between the $N = 2$ and 3 states. The $N = 2$ states are the ground state $\rm T_+$ (left panel) and the excited states $\rm T_0$ (middle panel) and S (right panel). Red and blue outlined arrows depict the tunneling of a spin-up and a spin-down electrons, respectively.

time it resides at $N = 2$ and at $N = 3$, respectively. The histogram of the filled time plotted in Fig. 1(c) shows a single exponential distribution with a time constant of $\tau_{\rm f} = 2.9$ ms, whereas the empty time exhibits a double exponential distribution with time constants of $\tau_{\rm e1} = 0.12$ ms and $\tau_{\rm e2} = 4.4$ ms, as shown in Fig. 1(d). From the statistics of the empty time, we deduce the transitions involved in the observed $\Delta I_{\rm QPC}$ as schematically indicated in Fig. 1(e). The $N = 2$ ground state is $\rm T_+$, while the $N = 3$ ground state is a doublet $\rm D_+$ with $S_z = +1/2$ at $B_\perp = 1.5$ T. This assignment of the ground states is consistent with the results of the ground state spectroscopy [12]. Since these ground states are nearly at resonance, a transition between them occurs, involving the dot–lead tunneling of spin-down electrons. The detuning from the resonance is estimated to be approximately 10 μeV by analyzing the statistics of the filled and empty times in Figs. 1(c) and 1(d) [12]. In addition, transitions from/to the excited states are allowed because the energy distribution of the 2DEG lead is thermally broadened. We calculate the single particle energies in our device and estimate the excitation energies from $\rm D_+$ to S and $\rm T_0$, and from $\rm T_+$ to the $N = 3$ quadruplet $\rm Q_{+3/2}$ with $S_z = +3/2$ to be 40 to 90 μeV [12] as shown in Fig. 1(e). For this excitation energy, the value of the Fermi distribution function ranges from 0.001 to 0.05 at 160 mK. The tunnel coupling for spin-up electrons is an order of magnitude larger than for spin-down electrons, owing to the spin filtering, as estimated later. Therefore, the transition rates from $\rm D_+$ to S, from $\rm D_+$ to $\rm T_0$, and from $\rm T_+$ to $\rm Q_{+3/2}$, are comparable to that for the transition between the ground states.

Next, we estimate the transition rates $\Gamma_{\rm T_+}$, $\Gamma_{\rm T_0}$, and $\Gamma_{\rm S}$, from $\rm T_+$, $\rm T_0$, and S, respectively, to $\rm D_+$, by considering the orbital effect. From the excited state spectroscopy [22] at $B_\perp = 0$ T, the tunnel coupling for p-orbital states is evaluated to be approximately three times higher than for s-orbital states in our device. Therefore, we assume $\Gamma_{\rm S} \approx 3\Gamma_{\rm T_0}$ because a spin-up electron tunnels into the p-orbital (s-orbital) for the transition from S ($\rm T_0$) to $\rm D_+$ [23]. From the time constants of the empty time in Fig. 1(d), we evaluate $\Gamma_{\rm T_0} = 1/\tau_{\rm e1} = 8.3$ kHz and $\Gamma_{\rm T_+} = 1/\tau_{\rm e2} = 230$ Hz, and estimate $\Gamma_{\rm S} \approx 25$ kHz. We assume that the transition of neither S to $\rm D_+$ nor $\rm Q_{+3/2}$ to $\rm T_+$ is observed in $\Delta I_{\rm QPC}$ because their transition rates are higher than the measurement bandwidth. The three spin-dependent transition rates $\Gamma_{\rm T_+}$, $\Gamma_{\rm T_0}$, and $\Gamma_{\rm S}$ are given by the spin filtering by edge states in combination with the orbital effect, and can be used for the ternary readout of $\rm T_+$, $\rm T_0$, and S. The tunnel couplings are estimated to be 9.8 kHz and 760 Hz for spin-up and spin-down electrons in the s-orbital state, respectively, by analyzing the statistics of the filled and empty times [12]. This difference arises from the edge-state spin filtering.

We perform the single-shot ternary spin readout by applying voltage pulses to gate P as schematically shown in Fig. 2(a). $\Delta I_{\rm QPC}$ and the dot state filling, as expected for the pulse sequence, are also shown. First, the QD is initialized to $\rm D_+$ by waiting for 50 ms, sufficient for relaxing to the ground state. Next, the gate voltage is stepped down for the $N = 2$ configuration. A spin-up electron preferentially tunnels out of the QD to the lead because of the spin filtering, creating either S or $\rm T_0$ in a ratio of approximately 3 to 1, owing to the orbital effect. These excited states stochastically relax to $\rm T_+$ in the waiting time $t_{\rm wait}$. Finally, to read out the $N = 2$ spin configuration, the QD is set to the resonance between $N = 2$ and 3 as in Fig. 1(b). This condition is optimized to obtain high readout fidelity [12]. The electron tunneling time gives rise to a delay in the buildup of the $N = 3$ level of $\Delta I_{\rm QPC}$. We set the threshold for the $N = 3$ state buildup time to be 0.1 ms and 0.5 ms to distinguish between S and $\rm T_0$ and between $\rm T_0$ and $\rm T_+$, respectively. The latter value is calculated using the transition rates and the spin relaxation time (shown later) [4], while the former value is given by the measurement bandwidth since the calculated optimal value of 62 μs is shorter than the bandwidth. We use the information about which time slot we observe the electron

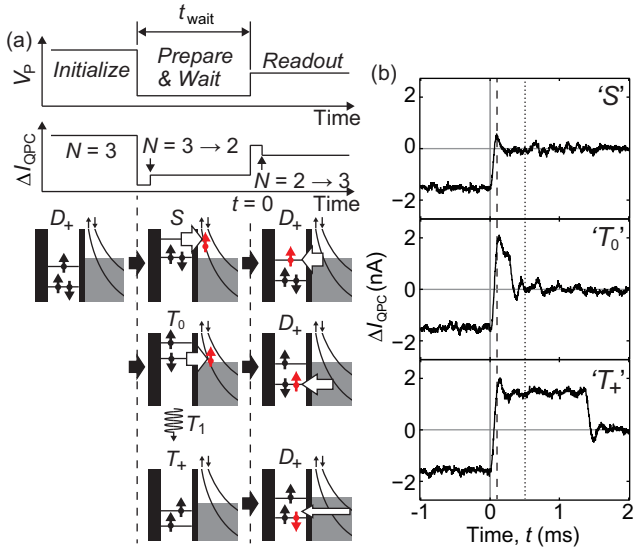

FIG. 2. (a) Schematics of (top) the voltage waveform applied to gate P; (middle) $\Delta I_{\rm QPC}$ in each stage; and (bottom) the possible QD states in each stage. Red arrows indicate electron spins tunneling into or out of the dot. (b) $\Delta I_{\rm QPC}$ in the readout stage for $t_{\rm wait} = 2.0$ ms [recognized as 'S' (top) and 'T_0' (middle)] and for $t_{\rm wait} = 20$ ms [recognized as 'T_+' (bottom)]. Vertical dashed and dotted lines indicate the positions of $t = 0.1$ ms and $t = 0.5$ ms, respectively.

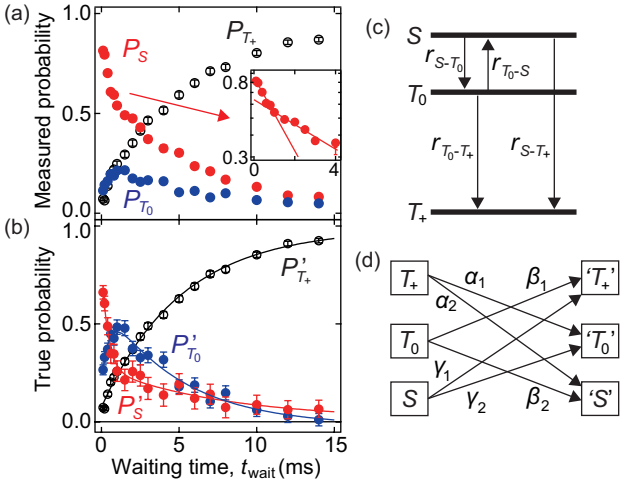

FIG. 3. (a) Measured probabilities $P_{\rm S}$, $P_{\rm T_0}$, and $P_{\rm T_+}$ of recognizing 'S' (red), 'T_0' (blue), and 'T_+' (black), respectively, as a function of $t_{\rm wait}$. Inset shows $P_{\rm S}$ for the $t_{\rm wait}$ range of 0 to 4 ms in the logarithmic scale. (b) True probabilities $P'_{\rm S}$, $P'_{\rm T_0}$, and $P'_{\rm T_+}$ of S (red), T_0 (blue), and T_+ (black), respectively, calculated using the measured probabilities in (a) and the transition rates. (c) Spin relaxation processes involved in the time evolutions of $P'_{\rm S}$, $P'_{\rm T_0}$, and $P'_{\rm T_+}$ in (b). (d) Definition of error rates α_1, α_2, β_1, β_2, γ_1, and γ_2.

loading event in the readout stage, at times $t < 0.1$ ms, 0.1 ms $\leq t < 0.5$ ms, or $t \geq 0.5$ ms, to identify the $N = 2$ state after $t_{\rm wait}$ as 'S', 'T_0', or 'T_+', respectively. Note that $Q_{+3/2}$ may also be created by loading a spin-up electron into T_+, but we ignore this tunneling process because $Q_{+3/2}$ quickly transits back to T_+ with a rate much higher than the measurement bandwidth.

Figure 2(b) shows the typical real-time traces of $\Delta I_{\rm QPC}$ measured for $t_{\rm wait} = 2.0$ ms (top and middle) and $t_{\rm wait} = 20$ ms (bottom). The QD is set to the above-mentioned readout stage at $t = 0$, at which $\Delta I_{\rm QPC}$ steps up because of the gate voltage change. We define $\Delta I_{\rm QPC} = 0$ nA for the $N = 3$ signal level at the readout stage. In this experiment, each event of single-electron tunneling changes $\Delta I_{\rm QPC}$ by 1.5 nA. In the top panel, $\Delta I_{\rm QPC}$ shows only a small spike of $\Delta I_{\rm QPC} = 0.5$ nA at $t = 0.1$ ms. This spike is caused by the gate voltage change and the cross-talk between measurement wires. Therefore, $\Delta I_{\rm QPC}$ remains at the $N = 3$ signal level throughout the readout stage without reaching the $N = 2$ signal level ($\Delta I_{\rm QPC} = 1.5$ nA). This shows that electron tunneling from $N = 2$ to 3 has occurred at $t < 0.1$ ms, which is faster than the measurement bandwidth. Thus, we recognize the $N = 2$ spin state before the readout stage as 'S'. In the middle panel, $\Delta I_{\rm QPC}$ shows a peak with a height of $\Delta I_{\rm QPC} = 2.0$ nA at $t = 0.1$ ms. This peak height is interpreted as a sum of the $N = 2$ signal level and the offset due to the crosstalk. Then $\Delta I_{\rm QPC}$ steps down to the $N = 3$ level at $t = 0.27$ ms. Therefore, the $N = 2$ spin state is recognized as 'T_0'. In the bottom panel, $\Delta I_{\rm QPC}$ stays at the $N = 2$ level for t up to 1.4 ms and then steps down to the $N = 3$ level, from which we recognize the $N = 2$ spin state as 'T_+'.

To confirm the validity of the readout scheme used here, we measure the spin relaxation of the excited states S and T_0. We obtain 1000 traces similar to those in Fig. 2(b) for different values of $t_{\rm wait}$. Figure 3(a) shows the measured probabilities, $P_{\rm S}$, $P_{\rm T_0}$, and $P_{\rm T_+}$ of recognizing 'S', 'T_0', and 'T_+', respectively, as a function of $t_{\rm wait}$. $P_{\rm S}$ shows a double exponential decay, while $P_{\rm T_+}$ increases single-exponentially. In contrast to these monotonic changes, $P_{\rm T_0}$ increases to approximately 0.2 with increasing $t_{\rm wait}$ up to 1.5 ms and then decreases for longer $t_{\rm wait}$ values. The qualitatively different $t_{\rm wait}$ dependencies of $P_{\rm S}$, $P_{\rm T_0}$, and $P_{\rm T_+}$ imply that we have successfully identified the three $N = 2$ spin states.

To understand the $t_{\rm wait}$ dependencies of the probabilities in Fig. 3(a), we estimate the true $N = 2$ state probabilities, $P'_{\rm S}$, $P'_{\rm T_0}$, and $P'_{\rm T_+}$, for S, T_0, and T_+, respectively. First, $P'_{\rm T_+}$ is obtained by rescaling $P_{\rm T_+}$ so that $P'_{\rm T_+} = 0$ at $t_{\rm wait} = 0$ because of the efficient spin filtering and $P'_{\rm T_+} = 1$ at $t_{\rm wait} \to \infty$ due to the spin relaxation. Next, we consider the readout error by which the true T_0 is misinterpreted as 'S'. Such an error occurs with the probability $p_{\rm err} \approx 60\%$ for $\Gamma_{\rm T_0} = 8.3$ kHz and the threshold of 0.1 ms. Thus, we obtain $P'_{\rm T_0} = P_{\rm T_0}/(1 - p_{\rm err})$ and $P'_{\rm S} = P_{\rm S} - P_{\rm T_0} p_{\rm err}/(1 - p_{\rm err})$.

The calculated $P'_{\rm S}$, $P'_{\rm T_0}$, and $P'_{\rm T_+}$ are shown in Fig.

3(b). P'_{T_0} (P'_{T_+}) is larger than P_{T_0} (P_{T_+}) in Fig. 3(a), whereas P'_{S} is smaller than P_{S}, though the t_{wait} dependence is similar for all. Note that P'_{S} is three times larger than P'_{T_0} when $t_{\mathrm{wait}} \to 0$ in Fig. 3(b), which is consistent with the ratio of the transition rates caused by the orbital effect. By fitting a double exponential function to P'_{S} and P'_{T_0}, we obtain time constants of $\tau_{\mathrm{S}1} = 0.42 \pm 0.08$ ms and $\tau_{\mathrm{S}2} = 7.8 \pm 2.4$ ms for P'_{S}, and $\tau_{\mathrm{T}_0 1} = 0.47 \pm 0.13$ ms and $\tau_{\mathrm{T}_0 2} = 4.9 \pm 0.7$ ms for P'_{T_0}. Because the decrease in P'_{S} and the increase in P'_{T_0} are comparable in both magnitude and time constant, we attribute $\tau_{\mathrm{S}1}$ and $\tau_{\mathrm{T}_0 1}$ to the spin relaxation from S to T_0. In addition, the finite value of P'_{S} at around $t_{\mathrm{wait}} = 1.5$ ms after S to T_0 relaxation implies the thermal equilibrium between S and T_0. Thus, we conclude that S and T_0 are nearly degenerate at $B_\perp = 1.5$ T. Note that we observe the S to T_0 relaxation without such a distinct feature of the thermal equilibrium at a slightly different $B_\perp$ of 1.6 T, at which the energy spacing of S and T_0 may be large [12].

To estimate the spin relaxation times among S, T_0, and T_+, we consider the relaxation processes illustrated in Fig. 3(c). We solve the rate equations for this model, and obtain spin relaxation times, $1/r_{\mathrm{S\text{-}T_0}} = 0.68 \pm 0.12$ ms, $1/r_{\mathrm{T_0\text{-}S}} = 1.4 \pm 0.2$ ms, and $1/r_{\mathrm{S\text{-}T_+}} = 2.2 \pm 1.1$ ms, for S to T_0, T_0 to S, and S to T_+ relaxations, respectively. We cannot obtain the accurate value of $1/r_{\mathrm{T_0\text{-}T_+}}$ for T_0 to T_+ relaxation, supposedly because T_0 to T_+ relaxation is suppressed by the efficient thermal excitation from T_0 to S. Such a measurement of the dynamics between the two excited spin states is an important application of the ternary spin readout. The spin relaxation times measured in our device are comparable to those reported for two-electron spins in GaAs single QDs [4, 5, 24]. However, in terms of the spin relaxation mechanism [25–27], faster relaxation from S to T_0 than from S to T_+ and from T_0 to T_+ is inconsistent with the facts that S and T_0 are not directly coupled by the spin–orbit interaction and that phonon emission is inefficient when S and T_0 are nearly degenerate at $B_\perp = 1.5$ T. The reason for this inconsistency is not yet cleared.

Finally, we discuss the readout fidelity of the ternary spin readout. We define the error rates α_1, α_2, β_1, β_2, γ_1, and γ_2, with which the true states (S, T_0, and T_+) are misinterpreted as wrong states as schematically shown in Fig. 3(d). We cannot experimentally determine all of these error rates because it is difficult to accurately evaluate the preparation fidelities of all true states. Instead, we experimentally obtain $\alpha_1 + \alpha_2 = 0.075 \pm 0.010$ and $\beta_2 = 0.52 \pm 0.02$, and calculate $\beta_1 = 0.019$, $\gamma_1 = 0.016$, and $\gamma_2 = 0.094$ [12]. Using these error rates, we obtain the readout fidelities of 89.0%, 46.6 ± 1.8%, and 92.5 ± 1.0%, for S, T_0, and T_+, respectively, with an average fidelity of 76.0 ± 0.9%. One reason for the low fidelity in the T_0 readout is that the measurement bandwidth is not large enough to clearly distinguish between S and T_0. Moreover, the orbital effect is unexpectedly much less efficient in this work than in a previous work [4]. The average fidelity may be raised to 89% if the orbital effect is as efficient as stated in the previous report [4] and the measurement bandwidth is increased using a radio-frequency QPC [28]. Note that, for the binary spin readout of $S_z = 0$ (S and T_0) and T_+ using only the spin filtering, we achieve the readout fidelity as high as 97% at $B_\perp = 1.6$ T [12], which is comparable to the highest value ever reported for gate-defined QDs [5, 29].

The ternary spin readout in this work may be widely applied to QDs in various material systems including silicon-based devices [2, 3, 29, 30], graphene [31], transition metal dichalcogenides [32], and topological insulators [33, 34], in which the spin filtering may work when QDs are coupled to spin-polarized chiral or helical edge states. Thus, this spin readout scheme may provide a new technique for exploring spin dynamics in QDs, and unlocks a path for implementing three-level qutrits in QDs.

We thank Y. Tokura for fruitful discussions. This work was supported by Grant-in-Aid for Young Scientists B (No. 15K17681, No. 25790006), Grants-in-Aid for Scientific Research A (No. 25246005, No. 16H02204) and S (No. 26220710), Innovative Areas "Nano Spin Conversion Science" (No. 26103004), Intelligence Advanced Research Projects Activity project "Multi-Qubit Coherent Operations" through Copenhagen University, MEXT Project for Developing Innovation Systems, QPEC, the University of Tokyo, CREST, Japan Science and Technology Agency (JST), and ImPACT Program of Council for Science, Technology and Innovation (Cabinet Office, Government of Japan).

* kiyama@sanken.osaka-u.ac.jp

[1] J. M. Elzerman, R. Hanson, L. H. W. van Beveren, B. Witkamp, L. M. K. Vandersypen, and L. P. Kouwenhoven, Nature **430**, 431 (2004).
[2] C. B. Simmons, J. R. Prance, B. J. Van Bael, T. S. Koh, Z. Shi, D. E. Savage, M. G. Lagally, R. Joynt, M. Friesen, S. N. Coppersmith, and M. A. Eriksson, Phys. Rev. Lett. **106**, 156804 (2011).
[3] C. H. Yang, A. Rossi, R. Ruskov, N. S. Lai, F. A. Mohiyaddin, S. Lee, C. Tahin, G. Klimeck, A. Morello, and A. S. Dzurak, Nat. Commun. **4**, 2069 (2013).
[4] R. Hanson, L. H. Willems van Beveren, I. T. Vink, J. M. Elzerman, W. J. M. Naber, F. H. L. Koppens, L. P. Kouwenhoven, and L. M. K. Vandersypen, Phys. Rev. Lett. **94**, 196802 (2005).
[5] T. Meunier, K.-J. Tielrooij, I. T. Vink, F. H. L. Koppens, H. P. Tranitz, W. Wegsheider, L. P. Kouwenhoven, and L. M. K. Vandersypen, Phys. Status Solidi (b) **243**, 3855 (2006).
[6] J. P. Dehollain, J. T. Muhonen, K. Y. Tan, A. Saraiva, D. N. Jamieson, A. S. Dzurak, and A. Morello, Phys. Rev. Lett. **112**, 236801 (2014).

[7] C. Barthel, D. J. Reilly, C. M. Marcus, M. P. Hanson, and A. C. Gossard, Phys. Rev. Lett. **103**, 160503 (2009).

[8] A. Muthukrishnan and C. R. Stroud, Phys. Rev. A **62**, 052309 (2000).

[9] B. P. Lanyon, M. Barbieri, M. P. Almeida, T. Jennewein, T. C. Ralph, K. J. Resch, G. J. Pryde, J. L. O'Brien, A. Gilchrist, and A. G. White, Nat. Phys. **5**, 134 (2009).

[10] M. Ciorga, A. S. Sachrajda, P. Hawrylak, C. Gould, P. Zawadzki, S. Jullian, Y. Feng, and Z. Wasilewski, Phys. Rev. B **61**, R16315 (2000).

[11] H. Kiyama, T. Fujita, S. Teraoka, A. Oiwa, and S. Tarucha, Appl. Phys. Lett. **104**, 263101 (2014).

[12] See Supplemental Material at for details on observation of the spin filtering by edge states, statistical analysis of the filled and empty times, numerical calculations of energy levels, spin relaxation times, ternary spin readout at $B_\perp = 1.6$ T, binary readout of $S_z = 0$ and T_+, and error rates of ternary spin readout, which includes Refs. [13–20].

[13] P. L. McEuen, E. B. Foxman, Jari Kinaret, U. Meirav, M. A. Kastner, N. S. Wingreen and S. J. Wind, Phys. Rev. B **45**, 11419(R) (1992).

[14] N. Watase, M. Hashisaka, K. Muraki, and T. Fujisawa, Jpn. J. Appl. Phys. **53**, 04EJ01 (2014).

[15] L. H. Willems van Beveren, R. Hanson, I. T. Vink, F. H. L. Koppens, L. P. Kouwenhoven, and L. M. K. Vandersypen, New. J. Phys. **7**, 182 (2005).

[16] A. Kogan, S. Amasha, D. Goldhaber-Gordon, G. Granger, M. A. Kastner, and H. Shtrikman, Phys. Rev. Lett. **93**, 166602 (2004).

[17] F. H. L. Koppens, C. Buizert, K. J. Tielrooij, I. T. Vink, K. C. Nowack, T. Meunier, L. P. Kouwenhoven, and L. M. K. Vandersypen, Nature **442**, 766 (2006).

[18] J. Yoneda, T. Otsuka, T. Nakajima, T. Takakura, T. Obata, M. Pioro-Ladrière, H. Lu, C. J. Palmstrøm, A. C. Gossard, and S. Tarucha, Phys. Rev. Lett. **113**, 267601 (2014).

[19] A. V. Madhav, and T. Chakraborty, Phys. Rev. B **49**, 8163 (1994).

[20] D. M. Zumbühl, C. M. Marcus, M. P. Hanson, and A. C. Gossard, Phys. Rev. Lett. **93**, 256801 (2004).

[21] H. Kiyama, T. Nakajima, S. Teraoka, A. Oiwa, and S. Tarucha, Phys. Rev. B **91**, 155302 (2015).

[22] J. M. Elzerman, R. Hanson, L. H. W. van Beveren, L. M. K. Vandersypen, and L. P. Kouwenhoven, Appl. Phys. Lett. **84**, 4617 (2004).

[23] The orbital effect may change as $B_\perp$ increases. Nevertheless, three times larger P'_S than P'_{T_0} at $t_{wait} \to 0$ in Fig. 3(b) supports the assumption that the orbital effect is not significantly changed by $B_\perp$ in our device.

[24] T. Meunier, I. T. Vink, L. H. Willems van Beveren, K.-J. Tielrooij, R. Hanson, F. H. L. Koppens, H. P. Tranitz, W. Wegscheider, L. P. Kouwenhoven, and L. M. K. Vandersypen, Phys. Rev. Lett. **98**, 126601 (2007).

[25] A. V. Khaetskii and Y. V. Nazarov, Phys. Rev. B **61**, 12639 (2000).

[26] U. Bockelmann, Phys. Rev. B **50**, 17271 (1994).

[27] S. Dickmann and P. Hawrylak, JETP Lett. **77**, 30 (2003).

[28] D. J. Reilly, C. M. Marcus, M. P. Hanson, and A. C. Gossard, Appl. Phys. Lett. **91**, 162101 (2007).

[29] E. Kawakami, P. Scarlino, D. R. Ward, F. R. Braakman, D. E. Savage, M. G. Lagally, M. Friesen, S. N. Coppersmith, M. A. Eriksson, and L. M. K. Vandersypen, Nat. Nanotechnol. **9**, 666 (2014).

[30] M. G. House, T. Kobayashi, B. Weber, S. J. Hile, T. F. Watson, J. van der Heijden, S. Rogge, and M. Y. Simmons, Nat. Commun. **6**, 8848 (2015).

[31] J. Güttinger, T. Frey, C. Stampfer, T. Ihn, and K. Ensslin, Phys. Rev. Lett. **105**, 116801 (2010).

[32] X.-X. Song, D. Liu, V. Mosallanejad, J. You, T.-Y. Han, D.-T. Chen, H.-O. Li, G. Cao, M. Xiao, G.-C. Guo, and G.-P. Guo, Nanoscale **7**, 16867 (2015).

[33] M. Koñig, S. Wiedmann, C. Brne, A. Roth, H. Buhmann, L. W.. Molenkamp, X.-L. Qi, and S.-C. Zhang, Science **318**, 766 (2007).

[34] I. Knez, R.-R. Du, and G. Sullivan, Phys. Rev. Lett. **107**, 136603 (2011).